Electron Spin Resonance Imaging and ATR−FTIR Study of Poly(acrylonitrile−butadiene−styrene) Containing a Hindered Amine Stabilizer and Thermally Treated at 353 K

Mikhail V. Motyakin and Shulamith Schlick*

Department of Chemistry, University of Detroit Mercy, Detroit, Michigan 48219

Received November 5, 2001

ABSTRACT: We present an electron spin resonance imaging (ESRI) study of spatial effects in the thermal degradation at 353 K of poly(acrylonitrile−butadiene−styrene) (ABS) containing 1 or 2% (w/w) Tinuvin 770 as the hindered amine stabilizer (HAS). The spatial distribution of the HAS-derived nitroxide radicals was obtained by 1D ESRI. Nondestructive ("virtual") slicing of the 2D spectral−spatial images resulted in a series of ESR spectra, which indicated the presence of nitroxide radicals in two distinct sites; their relative intensity varied with sample depth. The two spectral components were assigned to nitroxide radicals located in domains rich in butadiene (B) and in styrene−acrylonitrile (SAN), respectively. 1D and 2D ESRI allowed the study of chemical processes within distinct morphological domains as a function of sample depth and treatment time. Attenuated total reflectance (ATR)−FTIR spectroscopy of the outer layer (500 μm thick) of the polymer was used to follow the increase of the carbonyl concentration and the decrease of the butadiene peak with time of treatment. The ESRI and FTIR experiments showed that a larger Tinuvin 770 content in the polymer leads to *less* efficient stabilization. Improvement of the software for image reconstruction in 1D experiments enabled the visualization of an outer layer of thickness ≈500 μm that is less degradable than the rest of the sample and believed to be formed during sample preparation by injection molding.

Introduction

1D and 2D ESRI methods have been used in order to determine the spatial variation of nitroxide radicals formed during polymer degradation in the presence of hindered amine stabilizers (HAS). Imaging is based on encoding spatial information in the ESR spectra via magnetic field gradients.[1−3] By 1D ESRI it was possible to deduce the distribution of radicals along the gradient direction.[4,5] 2D spectral−spatial ESRI is important in order to determine nondestructively the spatial variation of the spectral line shapes along the same direction.[1,2,6−8]

Spatial details in degradation processes are important for predicting the behavior and lifetime of polymeric materials exposed to UV, high-energy irradiation, and thermal and mechanical stresses. The extent and the spatial variation of degradation depend on the rate of formation of unstable intermediates and on the transport rate of atmospheric oxygen. When the oxygen needed in degradation processes can be provided by diffusion from the atmosphere, oxidative degradation occurs through the entire sample thickness. If however the supply rate of oxygen is less than the amount that can be consumed, as is often the case in accelerated aging in the laboratory, only thin surface layers are degraded, and the sample interior is less affected; this is the diffusion-limited oxidation (DLO) regime.[9,10] The DLO concept implies that lifetimes of polymeric materials deduced from the study of *average* properties for samples involved in accelerated degradation cannot be used to estimate the durability of polymers in normal exposures and use. For this reason methods for measuring the spatial distribution of polymer properties due to degradation have been developed. Of these methods, density profiling[11] and modulus profiling[12,13] are destructive. In contrast, IR microscopy,[14,15] chemiluminescence imaging,[16−18] and ESRI are nondestructive.

Chart 1

(a) Repeat Units in ABS

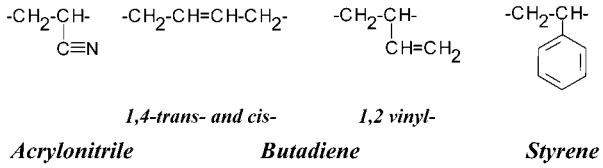

(b) Hindered Amine Stabilizer (HAS): Tinuvin 770

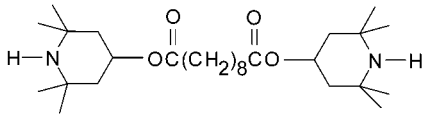

In previous papers we have described the application of ESRI for the study of photodegradation of ABS containing Tinuvin 770 as the HAS.[5−8] The repeat units in ABS and the amine are shown in Chart 1. Important details on the degradation process were based on the detection of two sites for the HAS-derived nitroxides, which were assigned to radicals located in domains differing in their monomer composition. The spatial distribution of the radical intensity obtained by 1D ESRI was heterogeneous as a result of irradiation using Xe (to mimic sunlight) or UVB (λ = 290−330 nm) sources; by contrast, the distribution of nitroxides produced during thermal degradation at 333 K was spatially homogeneous after 796 h of treatment.[6,7]

The stabilizing effect of hindered amines in photodegradation is widely documented; the amines are, however, considered somewhat less effective as thermal stabilizers.[19] During accelerated degradation, polymers are exposed not only to UV radiation but also to high

* Corresponding author. E-mail: schlicks@udmercy.edu.

10.1021/ma011919l CCC: $22.00
Published on Web 04/03/2002

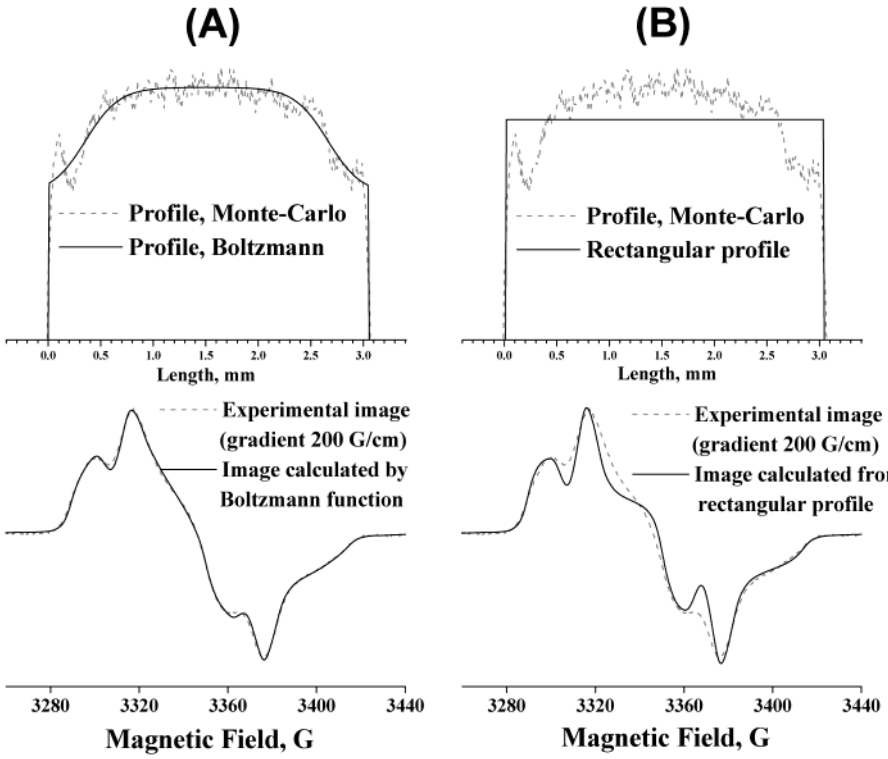

Figure 1. 1D ESRI of samples treated at 353 K for 456 h. Top in (A) and (B): comparison of nitroxide profiles deduced by the Monte Carlo method (- - -) and by analytical functions (—). Bottom in (A) and (B): experimental 1D image (- - -) and simulation by analytical functions (—). In (A) the Boltzmann function assumed the presence of a skin in the distribution, while in (B) a homogeneous (rectangular) distribution function was assumed. See text.

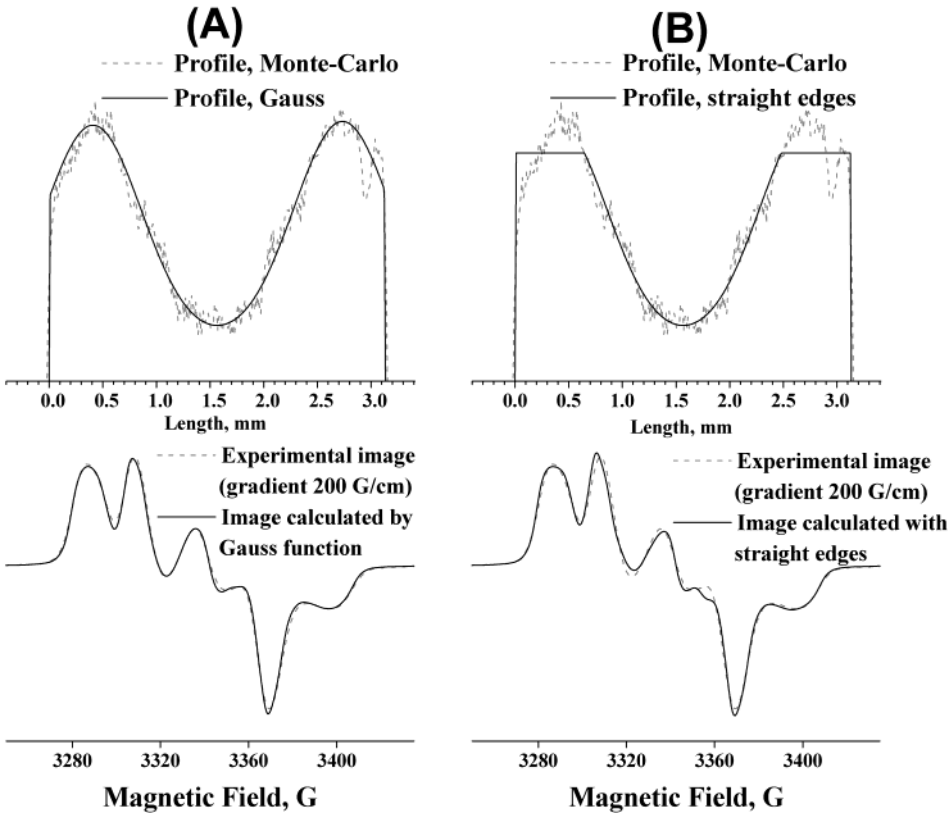

Figure 2. 1D ESRI of samples treated at 353 K for 3288 h. Top in (A) and (B): comparison of nitroxide profiles deduced by the Monte Carlo method (- - -) and by analytical functions (—). Bottom in (A) and (B): experimental 1D image (- - -) and simulation by analytical functions (—). In (A) the Gauss function assumed the presence of a maximum in the nitroxide distribution, while in (B) a skin with constant nitroxide distribution was assumed. See text.

temperatures. For this reason we have initiated a study by 1D and 2D spectral−spatial ESRI of the thermal degradation in ABS samples containing 1 or 2% (w/w) Tinuvin 770. The main objective of this study was to

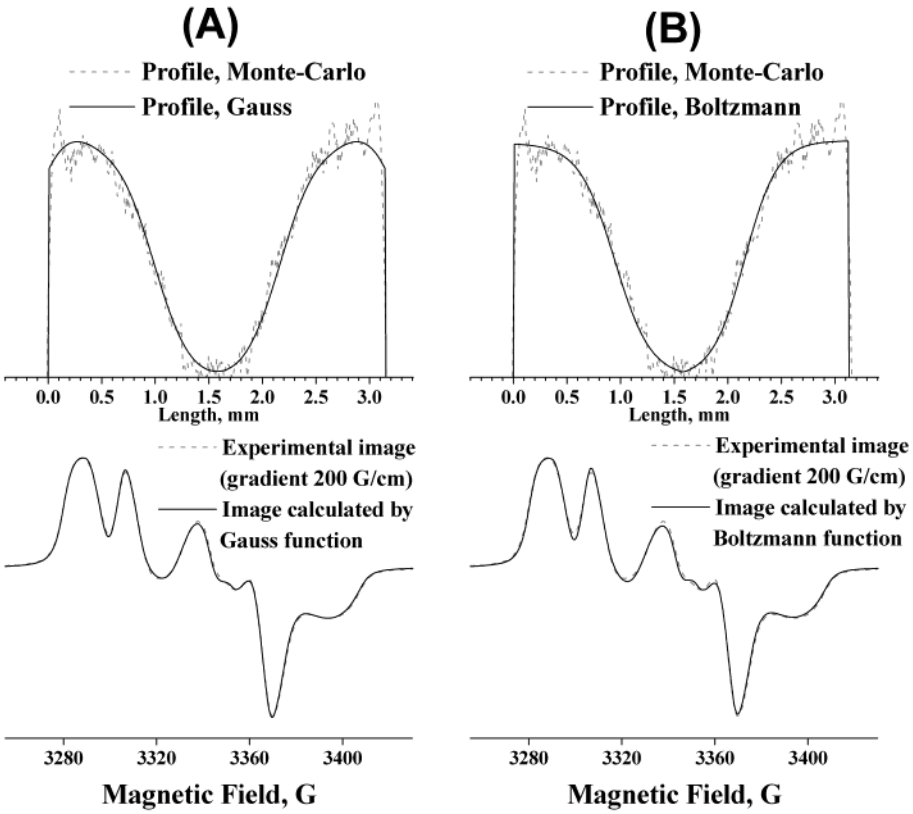

Figure 3. 1D ESRI of samples treated at 353 K for 5040 h. Top in (A) and (B): comparison of nitroxide profiles deduced by the Monte Carlo method (- - -) and by analytical functions (—). Bottom in (A) and (B): experimental 1D image (- - -) and simulation by analytical functions (—). In (A) the Gauss function assumed the presence of a maximum in the nitroxide distribution, while in (B) the nitroxide concentration was assumed to decrease from the outer edges to the sample interior. See text.

investigate the specific effect of hindered amine *light* stabilizers on the rate of *thermal* aging. The surprising result deduced from the ESRI study of thermal degradation at 393 K was that a larger Tinuvin 770 content in the polymer leads to less efficient stabilization.[8]

As will be clearly seen below, the onset of heterogeneous nitroxide distribution occurs after longer treatment times at 353 K compared to 393 K, but thermal degradation at 353 K is similar to that at 393 K in terms of the destabilizing effect of larger HAS content. In addition, 1D experiments of samples treated at 353 K enabled the visualization of an outer layer ("skin") of thickness ≈500 μm that is less degradable.

Experimental Section

Sample Preparation. Thermal degradation experiments were performed by heat treatment of ABS (Magnum 342 EZ from Dow Chemical Co., ≈10% (w/w) butadiene) doped with 1 or 2% (w/w) of (bis(2,2,6,6-tetramethyl-4-piperidinyl) sebacate), the HAS known as Tinuvin 770 from Ciba Specialty Chemicals (Chart 1). The polymer and the HAS were blended, shredded, and shaped into 10 cm × 10 cm × 0.3 cm plaques in an injection molding machine at 483 K. The plaques were thermally treated in a convection oven at 353 K. For the ESR imaging experiments, cylindrical samples 3−4 mm in diameter were cut from the plaques, and the samples were placed in the ESR resonator with the symmetry axis along the field gradient. Additional details have been reported.[5−8]

The sample notation used for describing the results is ABS0H, ABS1H, and ABS2H for ABS containing 0, 1, and 2% Tinuvin 770.

ESR Imaging and Data Acquisition. The 1D image is a convolution of the ESR spectrum in the absence of the gradient with the distribution of the paramagnetic centers along the gradient direction. These images were obtained with a field gradient of 200 G/cm. The ESR spectra and the 1D images were measured at 240 K to avoid the spatial dependence of the ESR signal.[5] Concentration profiles were obtained by simulation of the 1D image followed by deconvolution.

In previous studies,[5−7] we have deduced the concentration profiles by Fourier transform followed by optimization with the Monte Carlo (MC) procedure.[4] The disadvantage of this method is the high-frequency noise that is introduced when sharp edges in the profile are desirable. Despite the noise, profiles calculated by the MC procedure suggested a skin effect: edges of depth ≈500 μm contained a smaller concentration of nitroxides. To improve the quality of the profiles and validate the existence of the skin in noisy profiles, the intensity profile was fitted by an analytical function and convoluted with the ESR spectrum measured in the absence of the field gradient in order to simulate the 1D image. The best fit was obtained by variation of the analytical function (Gauss or Boltzmann, for example) and variation of the numerical parameters of the chosen function in order to get good agreement with the 1D image. Profiles deduced by the MC procedure and by various analytical functions are compared in Figures 1−3 for treatment times 456, 3288, and 5040 h, respectively. For treatment time of 456 h, Figure 1 clearly shows the improved fit to the experimental 1D image when a layer of lower nitroxide concentration is assumed (Figure 1A) compared to a homogeneous (flat) distribution (Figure 1B). For treatment time of 3288 h, the MC-derived profiles suggested a maximum nitroxide concentration at ≈500 μm from the edges; the assumption of a maximum in the simulation based on a Boltzmann analytical function (Figure 2A) reproduced better the 1D image compared to a "cut" profile (Figure 2B). After treatment time of 5040 h, the assumption of a maximum that shifts to the sample extremities compared to shorter treatment times (Figure 3A) led to a better fit to experimental data compared to a gradual decrease of the nitroxide concentration (Figure 3B). Figures 1−3 showed therefore that the use of analytical functions to simulate the 1D images led to

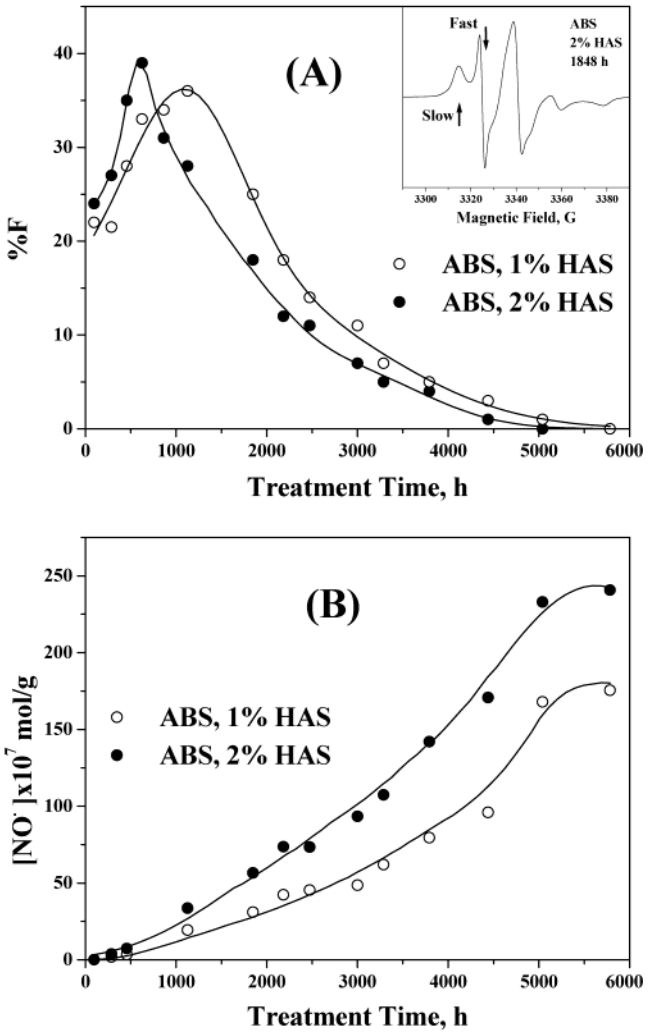

Figure 4. Relative concentration of the fast component, % F, in (A) and total nitroxide concentration in mol/g in (B) for whole ABS1H (○) and ABS2H (●) samples as a function of treatment time at 353 K. The solid lines in (A) and (B) were drawn by nonlinear regression. The inset in (A) is the ESR spectrum at 300 K of ABS2H after 1848 h of thermal treatment at 353 K; the low-field signals for the slow and fast components are indicated by arrows.

better fits with less noise and confirmed the existence of a polymer skin.

The 2D spectral−spatial images were reconstructed from a complete set of projections (typically 128) collected as a function of the magnetic field gradient, using a convoluted back-projection algorithm.[6−8] In the first step, the projections at the missing angles were assumed to be identical with the projection measured at the largest available angle. In the second stage, the projections at the missing angles were obtained by the projection slice algorithm (PSA)[20,21] with two iterations. The 2D images are displayed on a 128 × 128 grid.

ATR−FTIR Measurements. The spectra were measured with the Perkin-Elmer FTIR Spectrum 2000 spectrometer equipped with a horizontal attenuated total reflectance (HATR) accessory. The internal reflecting element (IRE) was a ZnSe crystal set at an incidence angle of 45°. Sections of thickness 500 μm were cut from the irradiated side of the cylindrical samples and dissolved in methylene chloride (from Fisher Scientific Co.). The polymer solution was poured directly on the ZnSe ATR crystal, and a polymer film was obtained by solvent evaporation. The film thickness was ≈100 μm, more than an order of magnitude larger than the maximum depth of penetration, d_p, calculated for $\lambda = 650$ cm^{-1}, by taking a refractive index of 2.4 for the ZnSe crystal, and a typical polymer refractive index in the range 1.20−1.40. The measurements were carried out in the spectral range 4000−700 cm^{-1}, with eight scans and 4 cm^{-1} resolution. The spectra were corrected for ATR using a zero contact angle, baseline corrected, and normalized to the 2238 cm^{-1} signal (acrylonitrile peak), which was assumed to be invariant during thermal treatment.[22] Additional details on the ATR−FTIR measurements have been reported.[23]

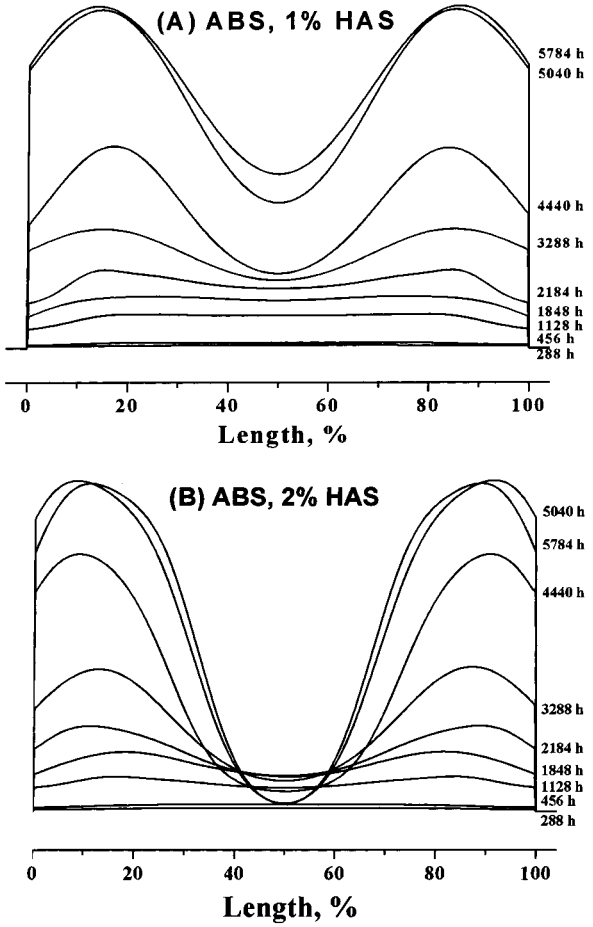

Figure 5. 1D concentration profiles in ABS1H for the indicated treatment times, normalized to the corresponding nitroxide concentration in whole samples shown in Figure 4B: (A) ABS1H; (B) ABS2H.

Results

Concentration and ESR Spectra of HAS-Derived Nitroxides. The ESR spectra at 300 K of the HAS-derived nitroxides in heat-treated ABS consist of a superposition of two components, from nitroxide radicals differing in their mobility: a fast component (F, extreme width ≈32 G) and a slow component (S, extreme width ≈64 G). A typical ESR spectrum at 300 K is shown in the inset of Figure 4 for ABS2H after 1848 h of thermal treatment. We assign the F and S components to nitroxides located respectively in low-T_g domains rich in linear polybutadiene (PB) and in high-T_g domains rich in poly(styrene-*co*-acrylonitrile) (SAN) or in cross-linked PB.[5−8] The two spectral components are due to the heterophasic nature of ABS.[14,24,25] As a result of polymer degradation, the F/S ratio varies with sample depth and treatment time; this variation provides the connection to the degradation and stabilization processes. The determination of the F/S ratio has been described.[5a]

The variation of % F and of the total nitroxide concentration in whole samples as a function of treat-

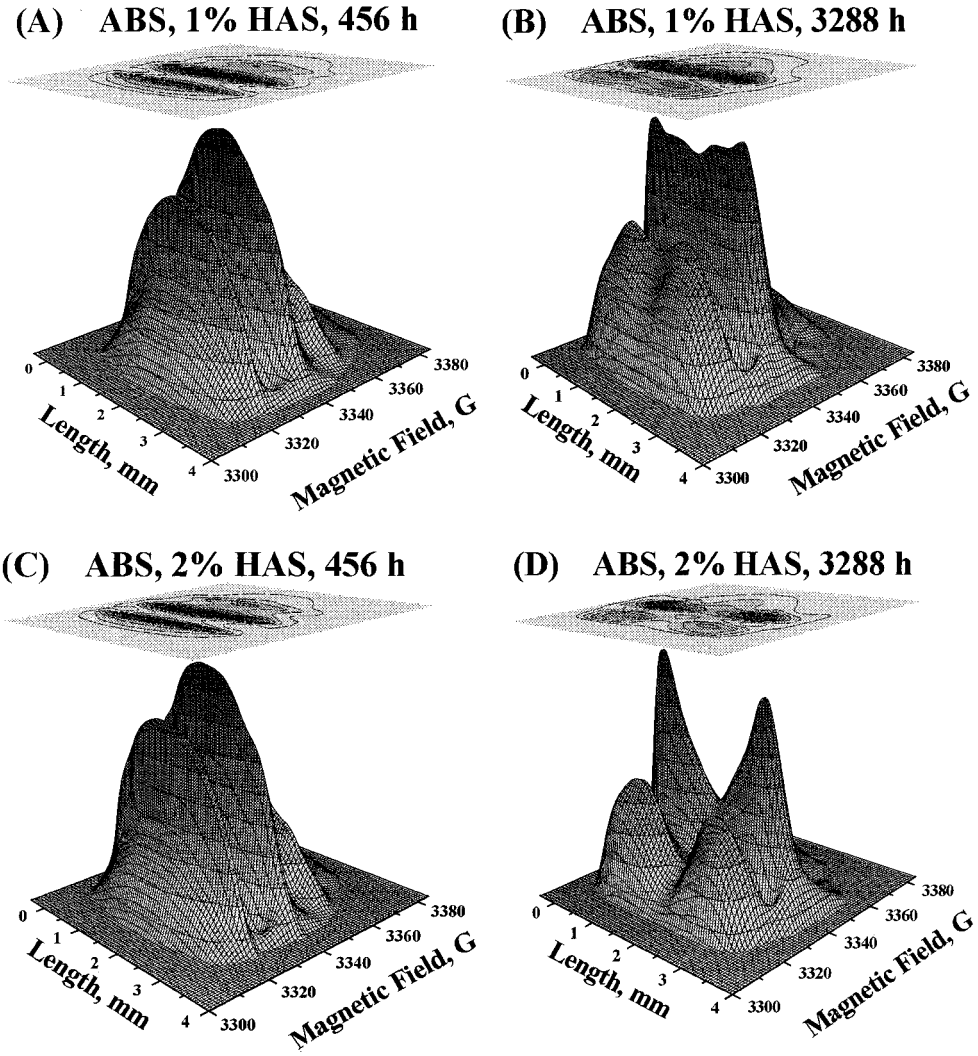

Figure 6. 2D spectral−spatial contour and perspective plots of HAS-derived nitroxides after 456 and 3288 h of thermal treatment at 353 K for ABS1H (A, B) and ABS2H (C, D), presented in absorption.

ment time, t, is shown in Figure 4. The relative intensity of the F component, Figure 4A, increases to a maximum at $t \approx 1400$ h for ABS1H and at $t \approx 800$ h for ABS2H, decreases with increasing treatment time, and becomes negligible for $t \geq 5000$ h in both cases. As in photodegradation, we assign the decrease of % F with treatment time to the consumption of the HAS-derived nitroxide radicals located in the butadiene-rich domains, because PB is more vulnerable to degradation compared to the styrene−acrylonitrile sequences in ABS.[26] This interpretation is supported by the ATR−IR of samples thermally treated at 393 K[8] and by results presented here in Figures 8 and 9.

The total intensity of HAS-derived nitroxides (Figure 4B), determined as described previously,[7] increases to a maximum for treatment time of ≈5500 h for both ABS1H and ABS2H. Similar maxima in nitroxide concentration have been detected in UV-exposed polymeric coatings containing 0.25−2% (w/w) HAS,[27] in ABS2H irradiated by a Xe source,[7] and in ABS thermally treated at 393 K.[8]

Concentration Profiles of Nitroxide. In Figure 5 we present the concentration profiles of nitroxides along the sample depth for ABS1H (A) and ABS2H (B) for the indicated treatment times. All profiles were normalized by the nitroxide concentration measured in whole samples, using data shown in Figure 4B. Spatially heterogeneous profiles due to DLO are clearly seen, especially for treatment times >1000 h. For a given treatment time, the heterogeneity of the 1D profiles is more pronounced for ABS2H. Also seen in Figure 5 is the presence of a layer of ≈500 μm with a lower nitroxide concentration.

2D Spectral−Spatial ESRI of Nitroxides. The 2D spectral−spatial perspective and contour plots of nitroxide radicals are given in Figure 6 for ABS1H and ABS2H, for treatment times of 456 and 3388 h. The ESR intensity is presented in absorption. The contour and perspective plots show clearly the distribution of the signal intensity, and the negligible signal intensity in the sample interior for ABS2H at long treatment times, as also seen in the concentration profiles deduced from 1D ESRI (Figure 5B).

The 2D images were virtually (nondestructively) sliced to give ESR spectra at various depths of the sample. These spectral slices reflect the spatial line shape variation and the relative intensity of each spectral component (F and S) as a function of sample depth. *Spectral profiling*, the depth variation of the F component, in ABS1H and ABS2H for treatment times 456, 2184, and 3288 h is presented in Figure 7. For the short treatment time (t = 456 h), the ESR spectra of the outer layers (thickness 400 μm) in contact with oxygen consist of two spectral components with % F ≈

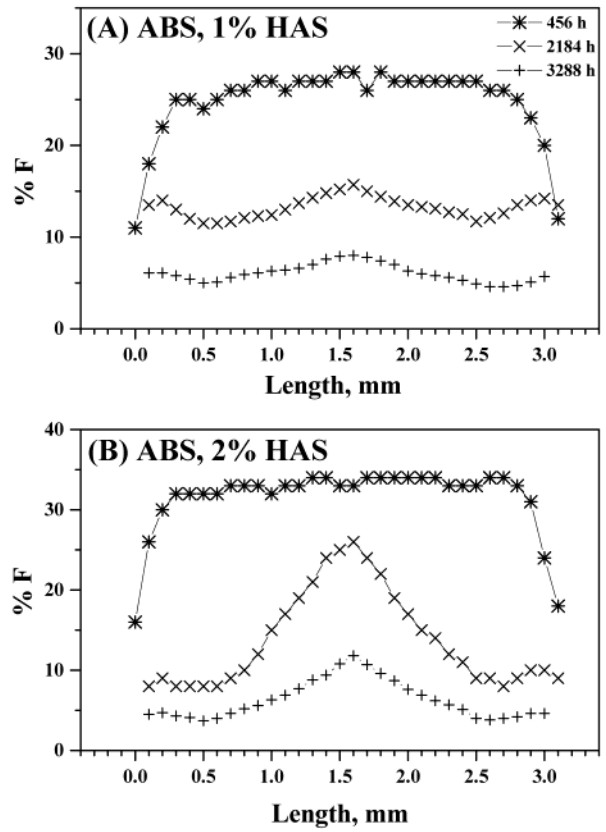

Figure 7. Spectral profiling: variation of % F with sample depth for ABS1H (A) and ABS2H (B) for the indicated treatment times at 353 K. The data were deduced from 100 μm thick virtual (nondestructive) slices in the corresponding 2D spectral−spatial ESR images.

10−25% for ABS1 and 15−33% for ABS2. After 2184 and 3288 h of treatment, % F decreases throughout the entire depth in ABS1H to % F ≈ 14 and 6%, respectively. For the same treatment times in ABS2H, % F decreases significantly at the sample extremities (to ≈8 and 4%, respectively), while the decrease in the center of the sample is less pronounced (to 26 and 10%, respectively). Corresponding % F depth variations were calculated for each treatment time.

Since the F component was assigned to nitroxides located in the PB-rich domains, the spectral profiling in Figure 7 emphasizes the changes that have occurred in these domains and can thus be also termed *elastomer phase profiling*.

ATR−FTIR Measurements. ATR−FTIR results are presented in Figures 8 and 9. Figure 8A shows spectra for the outer layer of thickness 500 μm on the outer layer for ABS1H and ABS2H after 5784 h of the treatment at 353 K. The spectra clearly indicate that the concentration of degradation products in the hydroxyl (3300−3600 cm^{-1}) and carbonyl (1650−1800 cm^{-1}) regions is higher in ABS2H compared to ABS1H. For the same treatment time, the butadiene peak intensity at 966 cm^{-1} decreases in the same order.

Changes in the carbonyl and butadiene regions respectively for ABS2H and ABS1H as a function of treatment time are given in Figure 8B,C. In the carbonyl region the peak for the sample that was not treated (0 h in Figure 8B) is assigned to the initial HAS. The increase of the carbonyl peak is observed only after ≈2000 h of thermal treatment, but the increase is smaller in ABS1H than in ABS2H. Similarly, the decrease of the butadiene peak at 966 cm^{-1} (Figure 8C) as a function of treatment time is more pronounced for ABS2H than for ABS1H.

The absorbance of the carbonyl (1731 cm^{-1}) and butadiene (966 cm^{-1}) peaks as a function of treatment time is presented for ABS0H, ABS1H, and ABS2H in Figure 9.

Discussion

In this section we will discuss the effect of sample preparation on the spatial dependence of chemical processes, assess the importance of HAS content on rate of ABS aging, and compare with results of thermal treatment for the same system at 393 K.

The Skin Effect. The extent of degradation due to UV irradiation and thermal treatment is expected to be homogeneous in the initial stages of the process and to decrease from the surface to the sample interior as aging progresses. This result is due to a combination of diffusion-limited oxidation and limited light penetration in UV irradiation.[28] For thermally treated samples, the temperature is constant through the entire sample during aging, and only the oxygen penetration through the sample must be considered.

Examination of the 1D profiles for ABS1H (Figure 5A) indicated however that a layer of ≈500 μm has a lower local concentration of nitroxide radicals. A similar skin is also seen for ABS2H (Figure 5B), but the layer is less pronounced and moves outward, to the sample extremities, for longer treatment times. The layer was not observed for ABS1H and ABS2H treated at 393 K;[8] it is possible that in that case the layer was thinner than the typical resolution in 1D experiments, ≈200 μm. It seems that the protective layer is more prominent in samples thermally treated at lower temperatures and/or for shorter times.

The % F deduced by 2D ESRI for 456 h of treatment, in both ABS1H and ABS2H, is lower in layers of thickness ≈500 μm at the sample extremities (Figure 7). For this time of treatment the nitroxide concentration is low (Figure 4) and the profiles are more homogeneous (Figure 5), suggesting early or negligible degradation. The unexpectedly low % F cannot therefore be due to the consumption of the stabilizer; instead, we propose that the amount of butadiene present at the sample extremities is lower than in the sample interior. According to this logic, there is more of the protective SAN component at the outside, a result that can be assigned to sample preparation by injection molding.

The existence of a skin where the degree of degradation is lower has been demonstrated for the early stages of degradation in polyethylene exposed to UV irradiation in the laboratory or in outdoor conditions.[28] The effect was observed for samples prepared by injection molding and not by compression molding. Several ideas were proposed for explaining the protective skin, among them blooming of the additive, surface cross-linking, and more degradation in the bulk after samples were released from the mold.

The data presented in Figures 5 and 8 for ABS1H and ABS2H do not reflect loss of the additive during sample preparation, as the skin is not seen clearly visible at higher aging temperature (393 K) when the effect would be enhanced.[8] The surface cross-linking hypothesis is also not valid for ABS, because it would reduce the diffusion of oxygen through the entire sample, yet spectral profiling (Figure 7) shows progressive decrease

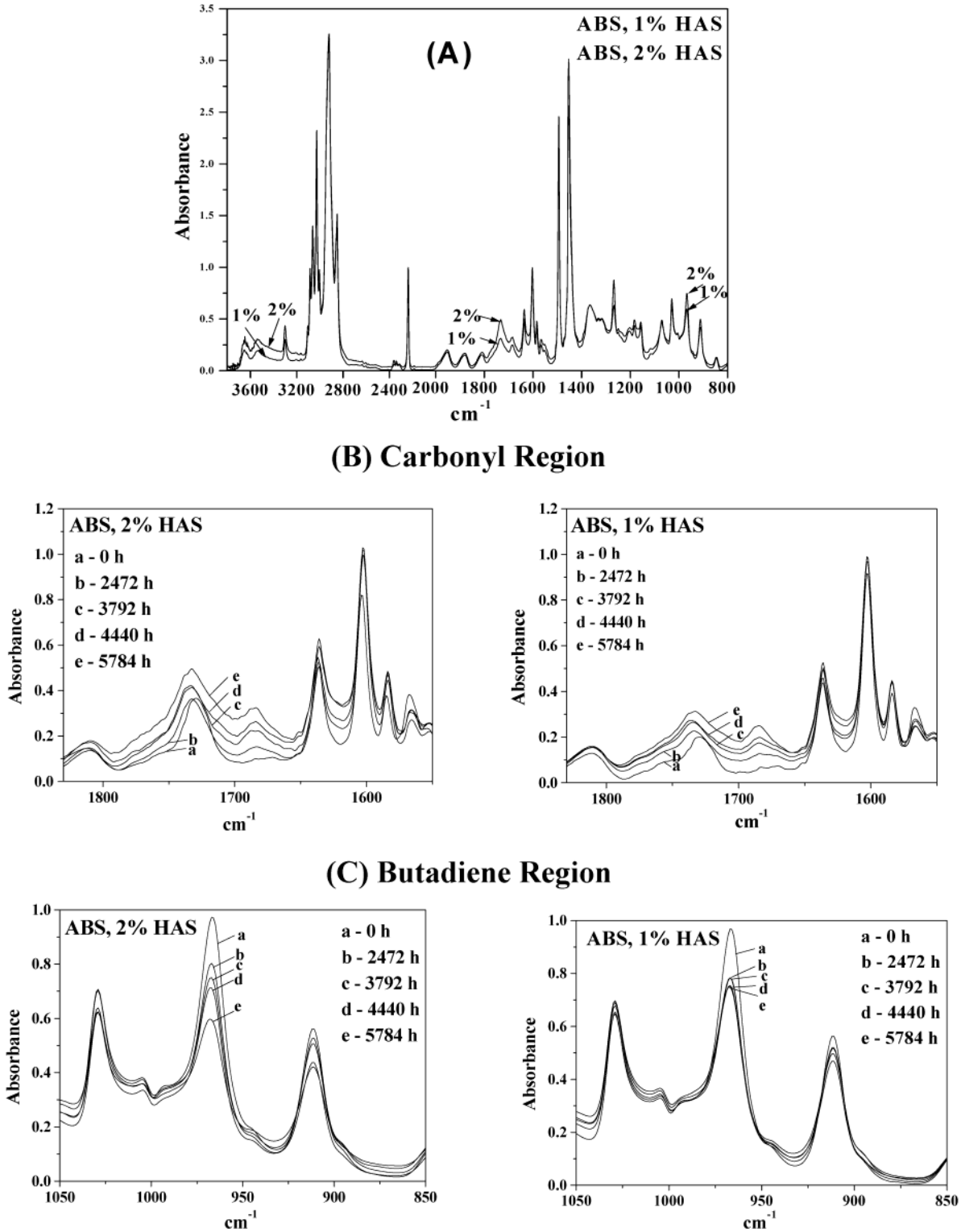

Figure 8. (A) ATR−FTIR spectra of the outer layer of thickness 500 μm in ABS1H and ABS2H treated for 5784 h at 353 K. (B) Changes in the carbonyl region for ABS2H and ABS1H. (C) Changes in the butadiene region for ABS2H and ABS1H. In (B) and (C) the treatment times were (a) 0, (b) 2472, (c) 3792, (d) 4440, and (e) 5784 h.

of the % F associated with the more degradable butadiene domains in the sample interior with progressive aging. It appears that the idea of a protective SAN layer formed by injection molding is the most plausible explanation for the skin effect. Moreover, details on the effect of sample preparation were detected in samples treated at lower temperatures and for shorter treatment times, because the aging process is slower. We emphasize that the interpretation of the skin effect is more straightforward in thermally treated samples, because we can exclude the spatial dependence of UV penetration, which must be considered in UV-treated samples, such as those reported in ref 28.

Effect of HAS Content on ABS Aging. The evolution of the 1D profiles shown in Figure 5 with increasing treatment times is indicative of the onset of DLO. The heterogeneity in the formation of nitroxide radicals is more pronounced for ABS2H (Figure 5B) compared to

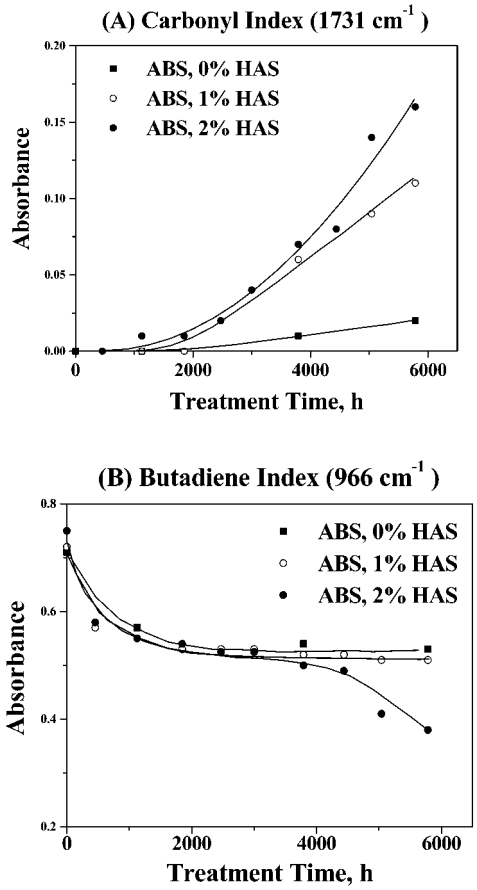

Figure 9. (A) Corrected absorbance in the carbonyl region (1731 cm^{-1}) as a function of treatment time at 353 K for an outer layer of thickness 500 μm in ABS0H, ABS1H, and ABS2H. The absorbance was obtained by subtracting the height of untreated samples from the corresponding heights of samples containing the same percentage of HAS. (B) Corrected absorbance in the 1,4-butadiene region (966 cm^{-1}) as a function of treatment time at 353 K for ABS0H, ABS1H, and ABS2H. The absorbance of the corrected spectra was plotted.

ABS1H (Figure 5A), as the nitroxide radicals are consumed in the center of the samples but not replaced during the aging process, because oxygen is consumed in the outside layers. Moreover, the skin is less pronounced in ABS2H as the treatment time increases, again a criterion for more advanced degradation.

A similar conclusions can be deduced from the spectral profiles deduced by 2D ESRI (Figure 7): If we exclude the skin layer for $t = 456$ h of treatment, the decrease of % F for ABS1H (Figure 7A) in the entire sample with increasing treatment time indicates the progressive disappearance of the polybutadiene component. For ABS2H (Figure 7B), however, % F is higher in the center and much lower in the sample extremities, an effect most clearly seen for $t = 2184$ h but also visible for $t = 3288$ h; more heterogeneous degradation and more advanced DLO conditions are suggested in ABS2H. Therefore, data presented in Figure 7 also indicate that a higher HAS content in ABS2H had a destabilizing effect compared to ABS1H.

Additional evidence for more degradation in ABS2H compared to ABS1H is reflected in the ATR−IR results (Figures 8 and 9): For a given treatment time, the carbonyl index (peak at 1731 cm^{-1}) is highest in ABS2H and lowest in ABS0H. The decrease of the butadiene index (peak at 966 cm^{-1}) is most evident in ABS2H. Taken together, the ESRI and IR data are in agreement, both suggesting that the rate of degradation is higher in the sample containing more HAS. The conclusion from the spectroscopic data are in agreement with the visual appearance of the samples: For the same treatment time, more discoloration and shape distortion were seen in ABS2H compared to ABS1H.

We note, however, that the ATR−FTIR data are not as informative as for thermal treatment at 393 K: For instance, the absorbance of the peak at 1731 cm^{-1} in ABS2H after 6000 h of treatment at 353 K (Figure 9A) is lower that that measured after 1896 h at 393 K;[8] the butadiene index (Figure 9B) is similar for ABS0H, ABS1H, and ABS2H up to $t = 4000$ h and decreases for ABS2H only after $t > 4500$ h. ESRI data shown in Figures 5−7 are capable of describing degradation processes in the early stages of aging, while IR spectra can be most informative for advanced stages of degradation.

We propose two types of processes that can explain the destabilizing effect of HAS. (1) Nitroxide radicals combine with polymer radicals P$^\bullet$ to form amino ethers, ⟩NOP, and can be regenerated by the reverse reaction ⟩NOP → ⟩NO$^\bullet$ + P$^\bullet$. Numerous studies have demonstrated the formation of ⟩NO$^\bullet$ and P$^\bullet$ by thermal decomposition of amino ethers above ambient temperature, even below 373 K.[29,30] The thermal sensitivity of the amino ethers might therefore be one reason for the lack of thermal stabilization by hindered amines. (2) Nitroxide radicals at elevated temperatures are known to be powerful abstractors of hydrogen.[30] Polymer-derived radicals can be produced by the hydrogen abstraction reaction, ⟩NO$^\bullet$ + PH → ⟩NOH + P$^\bullet$. While NOH is known to deactivate POO$^\bullet$ radicals and is considered part of the nitroxide regeneration mechanism, the formation of P$^\bullet$ by hydrogen abstraction may be an additional important contribution to further aging.

It is important to note that in many applications polymeric materials containing HAS are melt-processed at high temperatures; under these conditions thermal degradation due to the presence of the amine can be a significant factor.

In closing, we emphasize that 1D and 2D spectral−spatial ESRI methods are especially informative when applied to a polymer with a phase-separated morphology. The major advantage of these studies is the ability to visualize the variation of the HAS-derived nitroxide concentration due to degradation processes in distinct morphological domains within the sample depth and to deduce the profile of the elastomeric phase, shown here in Figure 7.

Conclusions

Electron spin resonance imaging (ESRI) was applied to the study of thermal degradation at 353 K of ABS containing 1 and 2% (w/w) Tinuvin 770 as the HAS.

Improvement of the software for image reconstruction in 1D experiments enabled the visualization of an outer skin of thickness ≈500 μm that was more resistant to degradation compared to the rest of the sample and is believed to form during sample preparation by injection molding.

The spatial distribution of the radical intensity obtained by 1D ESRI was heterogeneous for treatment times ≥1800 h for ABS1H and ≥1100 h for ABS2H. The spatial variation of the ESR spectra with sample depth was visualized by 2D spectral−spatial ESRI and used

to deduce the relative intensity of the nitroxide radicals in the two distinct sites along the sample depth. 1D and 2D ESRI allowed the determination of the extent of degradation and stabilization in distinct morphological domains as a function of sample depth with a resolution better than 200 μm.

The conclusions from ESRI were supported by FTIR-ATR spectroscopy of the outer layer (500 μm thick) of the polymer. Both ESRI and FTIR data indicated that larger Tinuvin 770 content in the polymer leads to higher degradation rates. Comparison of ESRI and IR methods emphasized the advantage of the ESRI method: its sensitivity to *early* events in the aging process.

Acknowledgment. This study was supported by the Polymers Program of NSF and by a University Research Grant from the Ford Motor Co. S. Schlick is grateful for a Fellowship from the Institute of Advanced Study, University of Bologna, in support of her 2001 sabbatical stay, and thanks Gian Franco Pedulli and Marco Lucarini for interesting discussions and hospitality in Bologna, Italy, where part of this manuscript was written. Special thanks are extended to Antonio Faucitano of the University of Pavia, Italy, for discussions and ideas on nitroxide reactivity at elevated temperatures.

References and Notes

(1) Schlick, S.; Pilar, J.; Kweon, S.-C.; Vacik, J.; Gao, Z.; Labsky, J. *Macromolecules* **1995**, *28*, 5780.
(2) Schlick, S.; Eagle, P.; Kruczala, K.; Pilar, J. In *Spatially Resolved Magnetic Resonance: Methods, Materials, Medicine, Biology, Rheology, Ecology, Hardware;* Blümler, P., Blümich, B., Botto, R., Fukushima, E., Eds.; Wiley-VCH: Weinheim, 1998; p 221.
(3) Degtyarev, E. N.; Schlick, S. *Langmuir* **1999**, *15*, 5040.
(4) (a) Lucarini, M.; Pedulli, G. F.; Borzatta, V.; Lelli, N. *Res. Chem. Intermed.* **1996**, *22*, 581. (b) Lucarini, M.; Pedulli, G. F. *Angew. Makromol. Chem.* **1997**, *252*, 179. (c) Franchi, P.; Lucarini, M.; Pedulli, G. F.; Bonora, M.; Vitali, M. *Macromol. Chem. Phys.* **2001**, *202*, 1246.
(5) (a) Motyakin, M. V.; Gerlock, J. L.; Schlick, S. *Macromolecules* **1999**, *32*, 5463. (b) In *Aging Studies and Lifetime Extension of Materials*; Mallinson, L. G., Ed.; Kluwer: New York, 2001; p 353.
(6) Kruczala, K.; Motyakin, M. V.; Schlick, S. *J. Phys. Chem. B* **2000**, *104*, 3387.
(7) Motyakin, M. V.; Schlick, S. *Macromolecules* **2001**, *34*, 2854.
(8) Motyakin, M. V.; Schlick, S. *Polym. Degrad. Stab.* **2002**, *76*, 25.
(9) Gillen, K. T.; Clough, R. L. *Polymer* **1992**, *33*, 4359.
(10) Billingham, N. C. In *Atmospheric Oxidation and Antioxidants;* Scott, G., Ed.; Elsevier: Amsterdam, 1993; Vol. II, Chapter 4, p 219.
(11) Gillen, K. T.; Clough, R. L.; Dhooge, N. J. *Polymer* **1986**, *27*, 225.
(12) Gillen, K. T.; Clough, R. L.; Quintana, C. A. *Polym. Degrad. Stab.* **1987**, *17*, 31.
(13) Gillen, K. T.; Clough, R. L.; Wise, J. In *Polymer Durability: Degradation, Stabilization and Lifetime Prediction*; Clough, R. G., Billingham, N. C., Gillen K. T., Eds.; *Adv. Chem. Ser. 249*; American Chemical Society: Washington, DC, 1996; Chapter 34, p 557.
(14) Jouan, X.; Gardette, J. L. *J. Polym. Sci., Part A: Polym. Chem.* **1991**, *29*, 685.
(15) Hoekstra, H. D.; Spoormaker, J. L.; Breen, J.; Andouin, L.; Verdu, J. *Polym. Degrad. Stab.* **1995**, *49*, 251.
(16) Celina, M.; George, G. A.; Lacey, D. J.; Billingham, N. C. *Polym. Degrad. Stab.* **1995**, *47*, 311.
(17) Matisova-Rychla, L.; Rychly, J. *Polym. Degrad. Stab.* **2000**, *67*, 515.
(18) Blakey, I.; George, G. A. *Macromolecules* **2001**, *34*, 1873.
(19) Scott, G. In *Atmospheric Oxidation and Antioxidants;* Scott, G., Ed.; Elsevier: Amsterdam, 1993; Vol. II, Chapter 5, p 279.
(20) Maltempo, M. M.; Eaton, S. S.; Eaton, G. R. In *EPR Imaging and In Vivo EPR*; Eaton S. S., Eaton, G. R., Ohno, K., Eds.; CRC Press: Boca Raton, FL, 1991; Chapter 14, p 145.
(21) Marek, A., unpublished work from this laboratory.
(22) Celina, M.; Wise, J.; Ottesen, D. K.; Gillen, K. T.; Clough, R. L. *Polym. Degrad. Stab.* **1998**, *60*, 493.
(23) Bokria, J. G.; Schlick, S. *Polymer*, in press.
(24) Daniels, E. S.; Dimonie, V. L.; El-Aasser, M. S.; Vanderhoff, J. W. *J. Appl. Polym. Sci.* **1990**, *41*, 2463.
(25) Kulich, D. M.; Gaggar, S. K. In *Polymer Durability: Degradation, Stabilization and Lifetime Prediction*; Clough, R. G., Billingham, N. C., Gillen, K. T., Eds.; *Adv. Chem. Ser. 249*; American Chemical Society: Washington, DC, 1996; Chapter 31, p 483.
(26) Carter, R. O. III; McCallum, J. B. *Polym. Degrad. Stab.* **1994**, *45*, 1.
(27) Gerlock, J. L.; Bauer, D. R.; Briggs, L. M. *Polym. Degrad. Stab.* **1986**, *14*, 53.
(28) De Bruijn, J. C. M. In *Polymer Durability: Degradation, Stabilization and Lifetime Prediction*; Clough, R. G., Billingham, N. C., Gillen K. T., Eds.; *Adv. Chem. Ser. 249*; American Chemical Society: Washington, DC, 1996; Chapter 36, p 599.
(29) Pospisil, J. *Adv. Polym. Sci.* **1995**, *124*, 87.
(30) Rozantsev, E. G.; Kagan, E. S.; Sholle, V. D.; Ivanov, V. B.; Smirnov, V. A. In *Polymer Stabilization and Degradation;* Klemchuk, P. P., Ed.; *ACS Symp. Ser. 280*; American Chemical Society: Washington, DC, 1985; Chapter 2, p 11.

MA011919L